ICARUS 114, 203–214 (1995)

Extinction Spectra of Corundum in the Wavelengths from UV to FIR

CHIYOE KOIKE

Kyoto Pharmaceutical University, Kyoto 607, Japan
E-mail: ckoike@jpnyitp.yukawa.kyoto-u.ac.jp

CHIHIRO KAITO

Ritsumeikan University, Kusatu 525, Japan

TETSUO YAMAMOTO

Hokkaido University, Sapporo 060, Japan

HIROSHI SHIBAI

Institute of Space and Astronautical Science, Sagamihara 229, Japan

SEIJI KIMURA

Ritsumeikan University, Kusatu 525, Japan

AND

HIROSHI SUTO

Communications Research Laboratory, Koganei 184, Japan

Received May 27, 1994; revised November 14, 1994

Extinction efficiency from UV to FIR wavelengths were measured for two kinds of γ-alumina particles; one is commercially available aerosil corundum particles, and the other is a combustion product. It is shown that the spectra showed very broad peaks around 13 μm and that the features agreed very well with those of the spectrum calculated using data of bulk amorphous γ-alumina. Complex refractive indices of the γ-alumina particles were deduced from dispersion relations and are presented both in figures and in numerical tables. A brief discussion is given on the possible presence of corundum dust in celestial objects and meteorites.

1. INTRODUCTION

Corundum (Al_2O_3) is one of the most refractory phases predicted to condense first from a gas of solar composition (Grossman 1972, Kornacki and Fegley 1984), but corundum has been found to be exceedingly rare in meteorites (Bar-Mathews *et al.* 1982, Anders *et al.* 1991). As a result, most experimental work on the primitive solar nebulae has been done on less refractory phases, such as hibonite ($CaAl_{12}O_{19}$) or anorthite feldspar ($CaAl_2Si_2O_8$). Recently, however, numerous corundum grains were found in the Murchison C2 chondrites (Anders *et al.* 1991, Virag *et al.* 1991). The analysis of grains by ion microprobe mass spectrometry indicated the existence of ^{26}Al and ^{16}O in the early Solar System (Anders *et al.* 1991, Virag *et al.* 1991). Furthermore, enrichment in ^{17}O and ^{26}Al found from Al_2O_3 grains in Orgueil C1 chondrite and Bishunpur LL3.1 chondrite suggests formation of Al_2O_3 grains in the atmospheres of red giant or AGB stars (Hutcheon *et al.* 1994, Huss *et al.* 1994). Corundum grains in meteorites give us a good clue to reveal processes in the early Solar System as well as those at presolar nebula stages.

The presence of corundum grains outside the Solar System is suggested from astronomical observations and theoretical calculations. Corundum grains were first identified in Mira variables; the broad 12-μm feature observed in the spectra of Mira variables without the 9.7-μm feature is identified as a band characteristic of alumina oxide particles (Vardya *et al.* 1986, Onaka *et al.* 1989). It is

0019-1035/95 $6.00

suggested theoretically that corundum grains may condense out of the gas ejected in the explosion of SN 1987A and Novae (Kozasa *et al.* 1989, 1991, Pearce and Evans 1984).

Optical constants of varieties of corundum grains are indispensable for analyzing the observed spectra, but they have not been obtained up to the present except those of bulk α- and γ-alumina. In this paper, we present the spectra of corundum grains measured in a wide wavelength region covering from UV to far infrared wavelengths, and the optical constants deduced by using the measured spectra and the dispersion relations.

2. EXPERIMENTS

Two types of samples of corundum grains were prepared: one is commercially available and the other is a combustion product. The samples were observed with Hitachi H-800 and H-7100 electron microscopes. The specimens were dispersed in ethyl alcohol and mounted on carbon-coated, perforated plastic films supported by standard copper electron-microscope grids. Electron microscopic (EM) images and electron diffraction (ED) patterns of corundum are shown in Figs. 1 and 2.

White commercially available corundum (hereafter referred to as "Alumina") from Nippon Aerosil Co., Ltd., was dissolved in aluminum chloride ($AlCl_3$) in a humid atmosphere at a high temperature. The commercial particles have a mean diameter of 200 Å and are disk-like in shape. There are many particles of 50- to 100-Å diameter, and several particles form aggregates as seen in Fig. 1. The size of each aggregate is about 200 Å. From the analysis of the ED patterns, the aerosil corundum (Alumina) particles are found to be predominantly composed of γ-alumina crystal with a small amount of α-alumina. Strong diffraction rings correspond to γ-alumina, and most of the weak diffraction rings correspond to α-alumina. Figure 3 shows a high-resolution electron microscopic image of these alumina particles. A particle with lattice fringes of 0.46 nm is γ-Al_2O_3. Some particles are

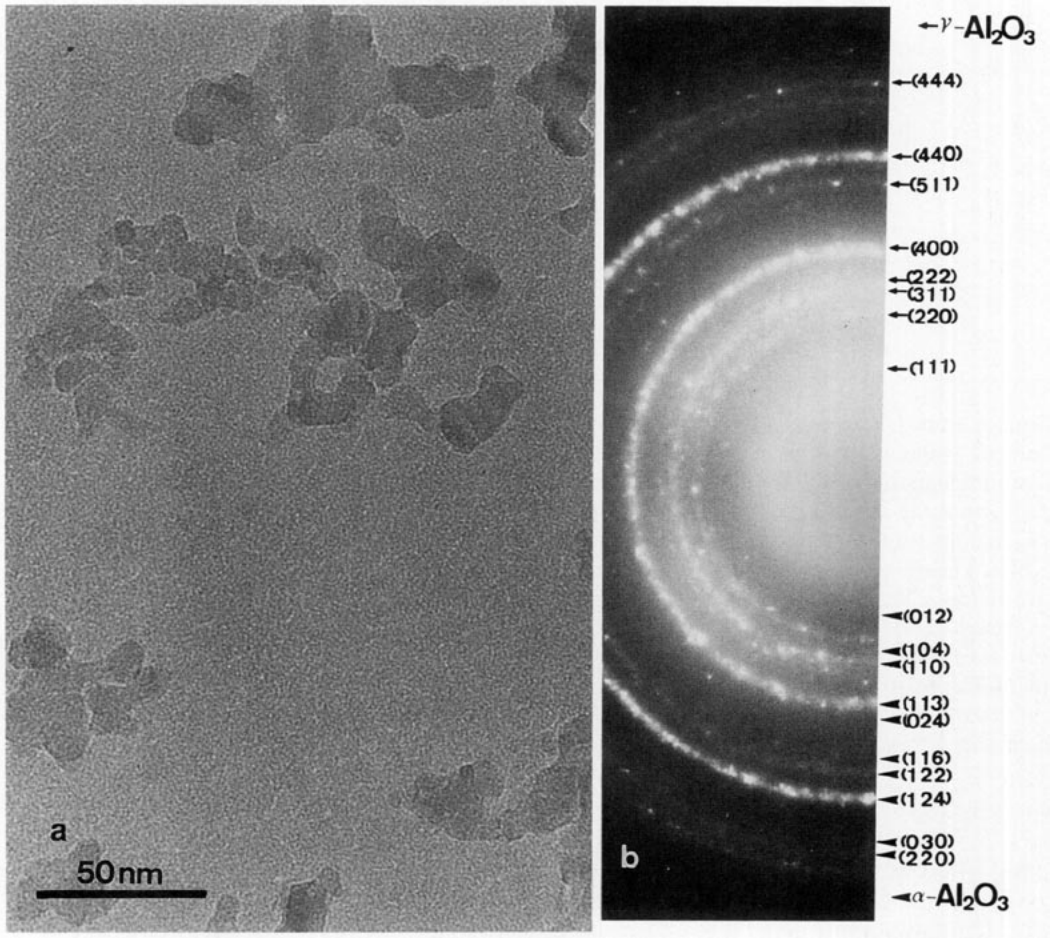

FIG. 1. TEM image and ED pattern of aerosil alumina particles (Alumina). The particles are disk-shaped and well dispersed. The size is about 50–100 Å for tiny particles and about 200 Å for particles consisting of a few tiny particles sticking to each other. The ED pattern shows strong rings characteristic of γ-alumina crystal and weak rings characteristic of α-alumina, indicating that the particles were composed predominantly of γ-alumina crystal and of a small amount of α-alumina.

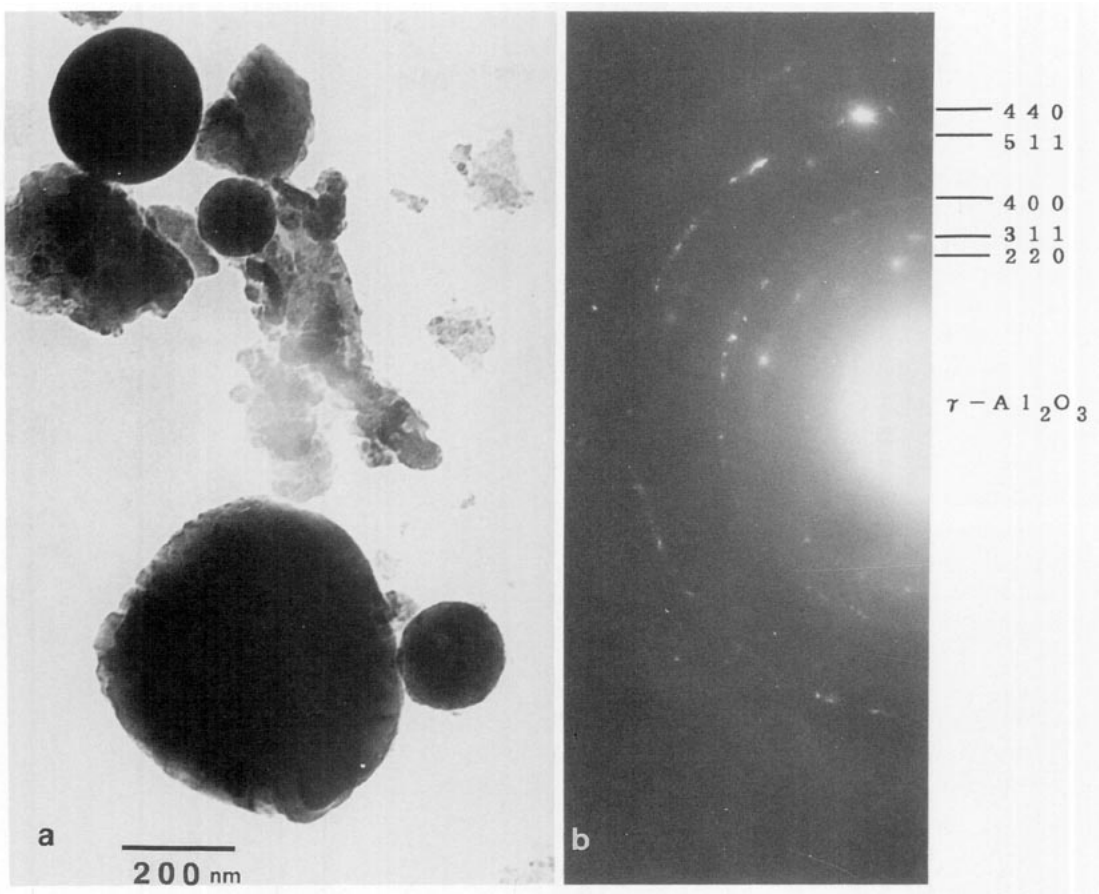

FIG. 2. TEM image and electron diffraction pattern of alumina particles obtained from combustion products (ISAS). The particles are a mixture of spherical and irregularly shaped ones. Spherical particles are 2000–3000 Å in size, irregular particles are about 200–300 Å, and those about 100 Å in size are numerous. The ED pattern indicates the presence of γ-alumina.

surrounded by a black contrast layer as indicated by arrows. The fringe seen at the periphery of the particle as indicated by an arrow (0.65 nm) corresponds to α-alumina. Therefore, the black contrast layers surrounding the particle may be due to α-alumina, which may be produced during dissolution by aluminum chloride. The inset at left in Fig. 3 partly shows a (110)γ fringe which corresponds to forbidden reflection in addition to a (220)γ fringe. This may indicate a phase transition process from γ to α phases. Experiments to investigate this phase transition are now in progress and will be published elsewhere.

Combustion product samples (hereafter referred to as "ISAS") are obtained from exhaust plumes of a solid-propellant rocket motor during ground firing tests at the Institute of Space and Astronautical Science (ISAS). They are gray and their mean size is about 0.5 μm. Particles with large size were removed by sedimentation in alcohol. The mean size of the remaining particles is about 0.3 μm. Both spherical and irregular-shaped particles are mixed in the sample as shown in the TEM image in Fig. 2. The sizes of the spherical particles are 1000–3000 Å, and those of the irregular shape are about 100–300 Å. In addition, particles of ~100 Å in size are fairly found. These samples were identified to be γ-alumina crystal by their ED pattern.

These samples were buried in KBr pellets or polyethylene sheets. The transmittance of the KBr pellets was measured with spectrometers of Shimadzu MPS-5000 in the UV–NIR wavelength region and with those of Shimadzu IR-27G from 2.5 to 25 μm. In the NIR wavelength region, we measured the transmittance of the KBr pellettes with a Fourier transform spectrometer (BOMEM Inc., Model DA3) at Communications Research Laboratory. In the far infrared region, the transmittance of the polyethylene sheets were measured with a Fourier transform spectrometer (BOMEM Inc., Model DA3) at ISAS.

3. RESULTS AND DISCUSSION

3.1. The Method of Deducing the Complex Refractive Index

The method of obtaining the complex refractive index of the sample particles is described in detail in Koike *et al.* (1989). Here we summarize it very briefly.

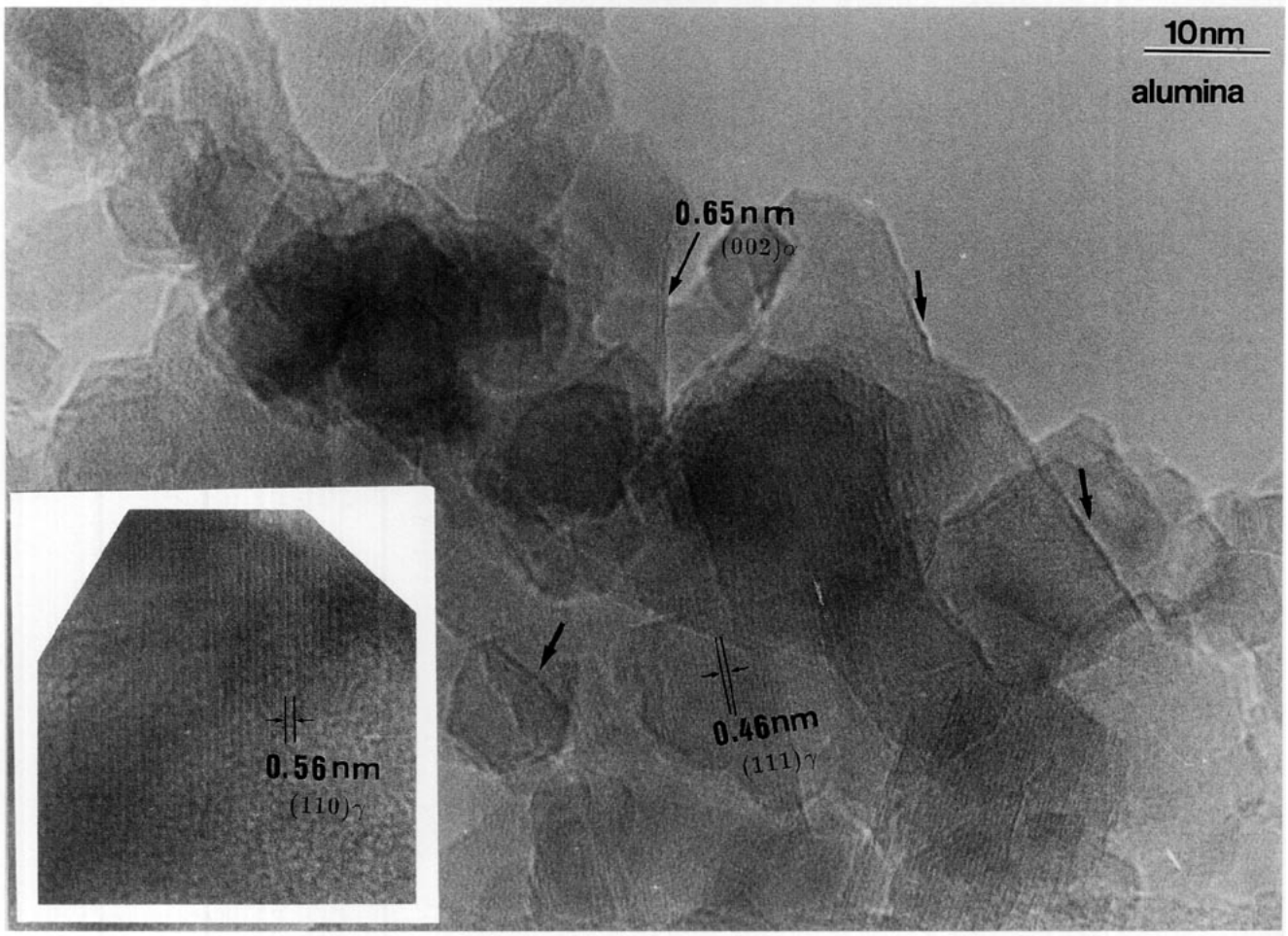

FIG. 3. High-resolution electron microscopic image of aerosil alumina particles.

For particles embedded in a medium (KBr pellets or polyethylene sheets), the extinction efficiency Q_{ext} of a sample particle of density ρ and radius a is obtained from the measurements of the transmittance T from the relation

$$\frac{Q_{ext}}{a} = \frac{4\rho S}{3M} \ln\left(\frac{1}{T}\right), \tag{1}$$

where S is the surface area of the KBr pellets or polyethylene sheets, and M is the total mass of sample included in the KBr pellets or polyethylene sheets. For a small particle that satisfies $2\pi a/\lambda \ll 1$ in a medium of refractive index n_0, Q_{ext} is related to the complex refractive index $m = n + ik$ of the particle as

$$\begin{aligned} Q_{ext}/a &= 4\left(\frac{2\pi n_0}{\lambda}\right) \mathrm{Im}\left[\frac{(m/n_0)^2 - 1}{(m/n_0)^2 + 2}\right] + \cdots \\ &= \frac{2\pi}{\lambda}\left[\frac{24 n k n_0^3}{(n^2 - k^2 + 2n_0^2)^2 + 4n^2k^2}\right] + \cdots, \end{aligned} \tag{2}$$

where n_0 is given by Heaton (1971) for KBr and by Mitsuishi *et al.* (1960) for polyethylene. Note that Q_{ext}/a is independent of particle radius a. From the measured Q_{ext}, the complex refractive index of a sample particle, $m = n + ik$, as a function of wavelength λ is obtained with the use of the dispersion relation as described later.

3.2. *Alumina*

Q_{ext}/a for Alumina particles in medium(KBr and polyethylene) is shown by the solid curve in Fig. 4, exhibiting a very broad peak at about 13 μm and a small shoulder at about 17–18 μm; the small shoulder appears at around 27 μm in polyethylene. As for the main peak, strictly speaking two types of peak features have been observed in many measurements done so far; one is a very broad peak at about 13 μm (12–13.5 μm), and the other is a double peak at about 12.4 and 13.3 μm. For the latter case the difference of the double peak is very subtle. The positions of these minor double peaks and small shoulders

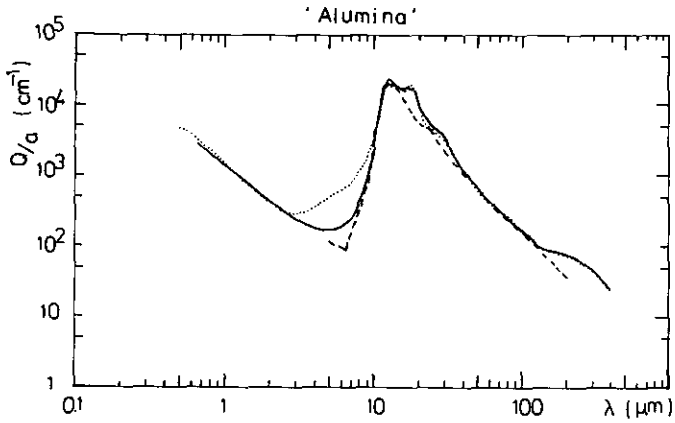

FIG. 4. Extinction efficiency of aerosil alumina particles (Alumina) embeded in KBr and polyethylene. The solid curve shows measured Q_{ext}/a, the dotted curve Q_{ext}/a calculated from the dispersion relations with the parameter values given in Table I, and the dashed curve Q_{ext}/a for γ-alumina calculated from the data of bulk γ-alumina (Eriksson *et al.* 1981).

are partly similar to those observed for forbidden modes of α-alumina (Barker 1963). As shown in Fig. 1, the ED pattern of aerosil alumina exhibits weak rings characteristic of α-alumina besides strong rings characteristic of γ-alumina, indicating that the particles were composed predominantly of γ-alumina crystal and of a small amount of α-alumina. The α-alumina may be partly transformed from γ-alumina as is shown in Fig. 3.

3.3. *"ISAS"*

Q_{ext}/a for combustion (ISAS) particles in medium(KBr and polyethylene) is shown by the solid curve in Fig. 5, which shows a very sharp peak as compared with that for alumina at about 13 μm (12.5–14 μm) and another

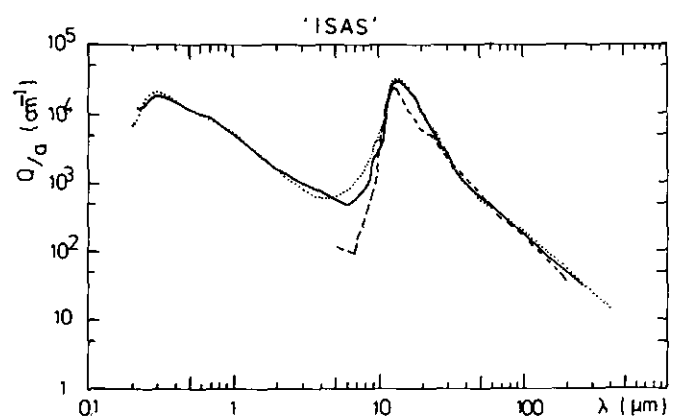

FIG. 5. Extinction efficiency of γ-alumina particles obtained from combustion products (ISAS) in KBr and polyethylene. The solid curve shows measured Q_{ext}/a, the dotted one Q_{ext}/a calculated from the dispersion relations. The dashed curve is the same as that in Fig. 4.

broad peak at about 3000 Å. As for the former peak, two types of the peak features also have been observed in many measurements: One is a very broad peak about 13 μm (12.5–14 μm), and the other is a double peak at about 12.4–12.9 and 13.5–13.9 μm. The peak positions of the double peaks varied from measurement to measurement. The difference between the two peaks is also very subtle as in Alumina. The features of these double peaks are similar to those of the weak forbidden modes of α-alumina measured for $E \perp C$ axis (Barker 1963). However, the ED pattern of the ISAS alumina shows the characteristic rings of only γ-alumina, so the double feature may be due to very small amount of partially degenerated γ-alumina.

3.4. *Comparison with the Data of Bulk Alumina*

There are many types of corundum denoted by α, β, γ, δ, χ, θ, κ, and η, whose crystalline structure is as follows: α, rhombohedral; β, hexagonal; γ and δ, tetragonal; χ, cubic?; θ, monoclinic; κ, orthorhombic system; and η, cubic system (Tanabe *et al.* 1993). The most common crystal lattice of Al_2O_3 is respectively referred to as α-Al_2O_3, sapphire, corundum, or alumina. We used here α-, β-, γ-, ··· -alumina.

For bulk α-alumina, the optical constants have been published (Barker 1963, Toon and Pollack 1976), which were deduced from the reflectance measurements using dispersion equations (Barker 1963). α-Alumina is a uniaxial crystal with the trigonal crystal system (Barker 1963). Although it is very difficult to blend the parameters of the two axes, sharp peaks appear at 13, 16, 21, and 26 μm in vacuum upon taking the average of Q_{ext} of the two axes as shown in Pearce and Evans (1984). Among the four peaks, the strongest are those at 13 and 21 μm. These features are clearly different from those of our data.

Eriksson *et al.* (1981) deduced the optical constants of a γ-alumina film formed by evaporation of alumina from the transmittance and reflectance measurements with the use the Kramers–Kronig relation. Their film was amorphous with γ-structure. For comparison with our data, we read out the optical constants from their figure. The results are shown in Figs. 4 and 5. The dashed curves indicate a Q_{ext}/a spectrum in the medium (KBr and polyethylene) calculated using the optical constants given by Eriksson *et al.* (1981). The spectrum shows a sharp peak at about 13 μm and a shoulder at about 25 μm.

Although our samples are crystalline γ-alumina, the features of both amorphous γ-alumina and our samples agree well as a whole except for the peaks at about 17–18 and 27 μm. The Alumina and ISAS spectra show much broader peaks than the alumina film. For the wide trough around 6 μm, the Alumina spectra fit better to that of amorphous γ-alumina (dashed curve) than to that of the ISAS. In the far infrared region, on the other hand, the

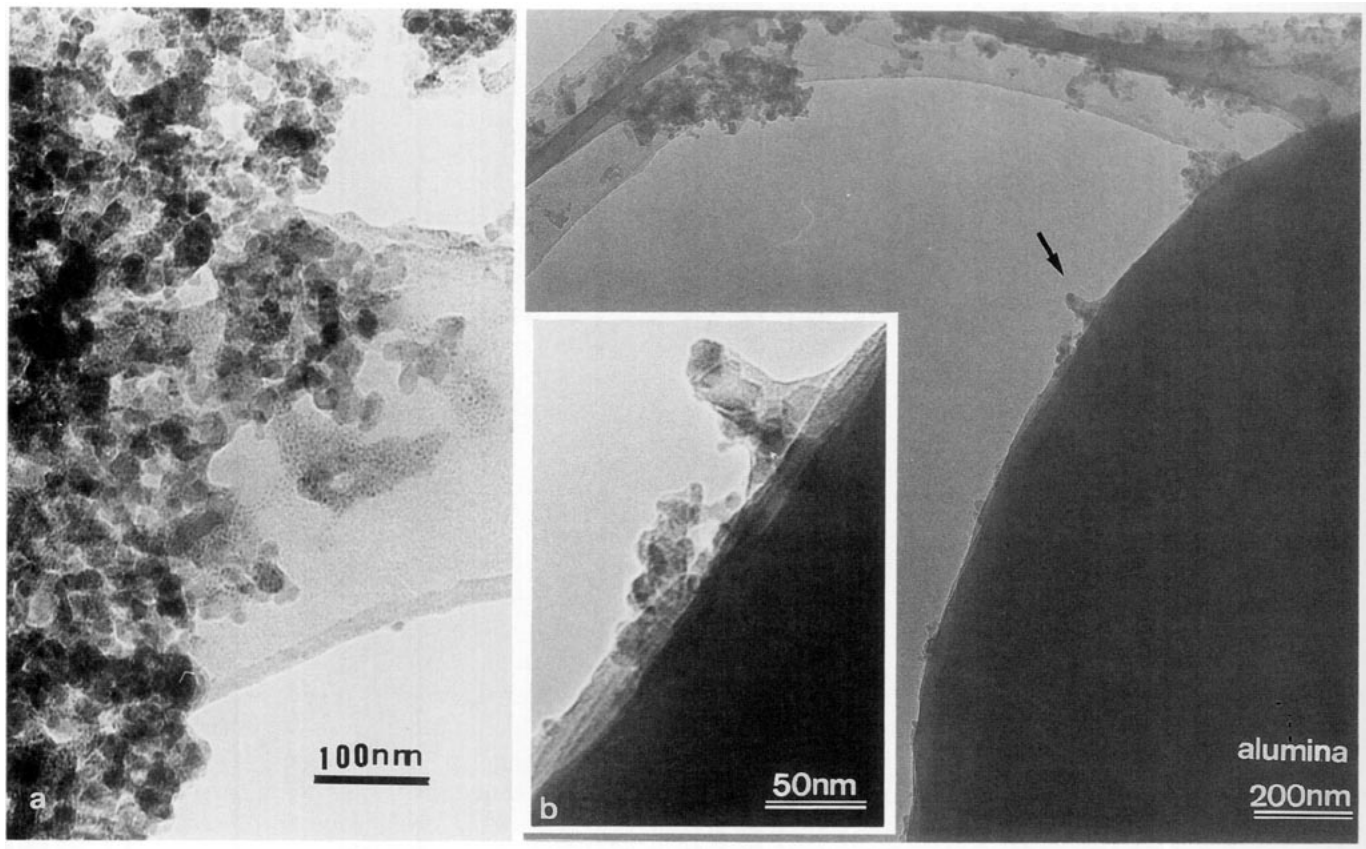

FIG. 6. TEM images of aerosil alumina particles (Alumina) among KBr particles (a) and polyethylene particles (b). The inset is an enlargement of the area indicated by an arrow in (b). The sample particles are well dispersed among KBr particles. A few particles stick on the surface of the polyethylene particle.

spectra of both samples Alumina and ISAS, especially that of ISAS, agree well with the spectrum of the amorphous γ-alumina.

It should be pointed out that, in general, such good agreement of the spectra of fine mineral particles with those of bulk in the FIR region is very rare. For other minerals such as magnetite, fused quartz, forsterite, and calcite, the measured spectrum of fine particles and the spectrum calculated with the use of bulk solid do not agree so well in the far infrared (Koike *et al.* 1981, Suto *et al.* 1992). One of the reasons for the disagreement might be due to the particle-aggregation effect (Koike *et al.* 1994).

To see this effect, we observed our samples in KBr and polyethylene powder by TEM. The TEM images are shown in Fig. 6. In KBr powder (Fig. 6a), the Alumina particles are surrounded by tiny KBr particles and isolated from each other, and in polyethylene powder (Fig. 6a), only a few Alumina particles are stuck to the surface of a polyethylene sphere. Thus the Alumina particles are rather well dispersed in the pressed KBr pellets and polyethylene sheets. This confirms the agreement of their spectra with those of bulk data. The agreement between the spectra calculated from the bulk data and those of Alumina and ISAS particles indicates that the difference of the shape (disk-like and spherical, respectively) and particle size (200 Å and 0.3 μm, respectively) has no appreciable effect on the spectral properties from UV to FIR wavelengths of ~100 μm.

3.5. *Optical Constants of γ-Alumina Crystal*

We determine the refractive indices of our samples, crystalline γ-alumina, using the measured extinction efficiency Q_{ext} and the dispersion relations (Pollack *et al.* 1973, Koike *et al.* 1989) given by

$$n^2 - k^2 = \varepsilon_\infty + \sum_j \frac{2P_j\Gamma_j}{\lambda_j} \frac{\lambda^2(\lambda^2 - \lambda_j^2)}{(\lambda^2 - \lambda_j^2)^2 + \Gamma_j^2\lambda^2}, \tag{3}$$

$$2nk = \sum_j \frac{2P_j\Gamma_j^2\lambda^3}{\lambda_j} \frac{1}{(\lambda^2 - \lambda_j^2)^2 + \Gamma_j^2\lambda^2}, \tag{4}$$

where the oscillator parameters λ_j, ρ_j, and Γ_j denote the wavelength, strength, and width of the jth oscillator, re-

TABLE I

Oscillator Parameters in the Dispersion Relations for "Alumina" and "ISAS" Spectra

'Alumina' ($j_{max} = 10$)			'ISAS' ($j_{max} = 13$)		
λ_j	P_j	Γ_j	λ_j	P_j	Γ_j
0.40	0.021	0.50	0.20	0.002	0.20
4.00	0.002	3.50	0.29	0.070	0.15
12.0	0.50	1.00	0.45	0.035	0.80
13.0	0.50	1.00	0.90	0.005	0.60
14.6	1.1	2.80	9.50	0.030	0.30
17.5	0.40	4.0	12.80	0.30	1.40
20.5	4.0	4.5	14.40	1.00	3.60
29.0	3.0	17.0	17.00	1.5	4.30
80.0	0.20	45.0	20.0	2.0	4.80
220.0	0.35	250.0	22.0	2.5	5.0
			27.0	5.1	7.0
			32.0	2.0	15.5
			60.0	0.65	100.0

spectively, while ε_∞ is the dielectric constant at short wavelengths and its value is 2.4 (Eriksson *et al.* 1981). The oscillator parameters are adjusted by Mie calculations of Q_{ext}/a with varying the parameter values until a fit is achieved to the measured Q_{ext}/a. The best-fit parameter sets for Alumina and ISAS are given in Table I. It is found that parts of the parameter λ_j for mid-infrared region are nearly same as those of forbidden modes of α-alumina (Barker 1963).

The complex refractive indices $m = n + ik$ are determined with use of the oscillator parameters given in Table I and are illustrated by solid curves in Figs. 7 and 8. For comparison n and k of amorphous γ-alumina read out from the figure in Eriksson *et al.* (1981) are also shown by dashed curves in Figs. 7 and 8. The numerical results are given in Tables A1 and A2 in Appendix. The n values from the UV wavelength region to about 20 μm for Alumina and ISAS are very nearly identical. In the region of wavelengths longer than 20 μm, on the other hand, the values of n and k differ between the samples, implying that these values vary with crystalline type and particle size. Q_{ext} in KBr and polyethylene calculated by using n and k in Table A1 is shown by the dotted curves in Figs. 4 and 5. It has been found that, even for a wide range of the values of the oscillator parameters, the trough in the spectrum for Alumina at about 6 μm has not been fully fitted in contrast with that for ISAS. This may be due to a small amount of α-alumina contained in Alumina as is suggested from the ED pattern (see Section 3.2 and Fig. 3).

4. SUMMARY: POSSIBLE PRESENCE OF ALUMINA DUST IN ASTRONOMICAL ENVIRONMENT

The presence of alumina grains has been found or suggested in various astronomical objects as listed in Table II. Here, we briefly summarize the possible presence of Al_2O_3 grains in meteorites, IDPs, circumstellar dust, and SN 1987A ejecta for the future spectral identification and specification of Al_2O_3 grains in celestial objects with the use of the optical constants obtained so far and in this paper.

4.1. Meteorites

Condensation theories (e.g., Grossman 1972, Yamamoto and Hasegawa 1977) predict that corundum had condensed first and later reacted with the cooling gas at a lower temperature to form another phase. Corundum act as a good probe to verify the condensation theory. Bar-Matthews *et al.* (1982) found a corundum-rich inclusion composed of corundum, hibonite, and perovskite in Murchison chondrites. Their SEM micrographs of the inclu-

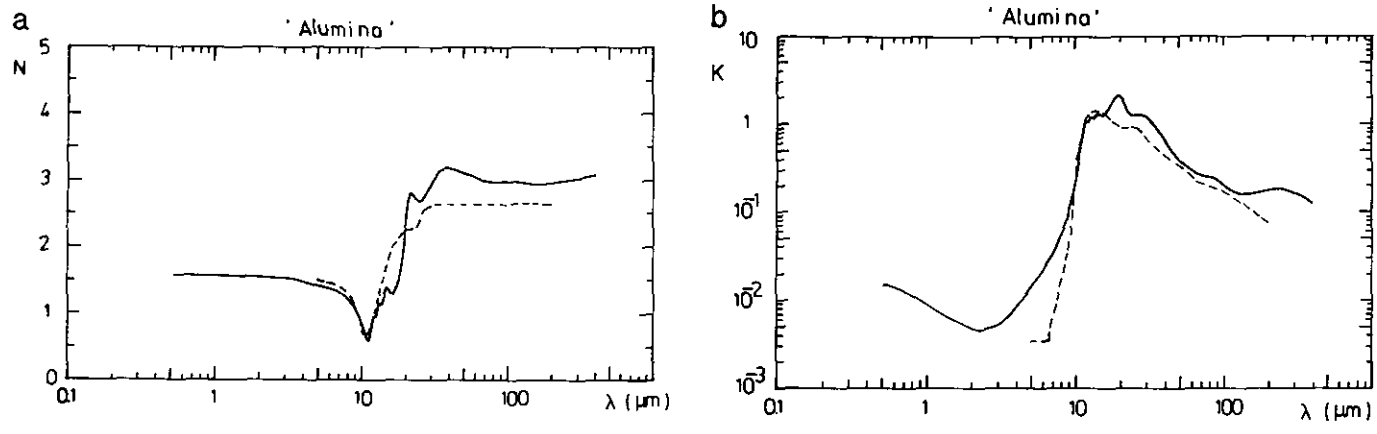

FIG. 7. The refractive indices n (a) and k (b) of aerosil alumina particles (Alumina). Those of γ-alumina (Eriksson *et al.* 1981) are shown by the dashed curve.

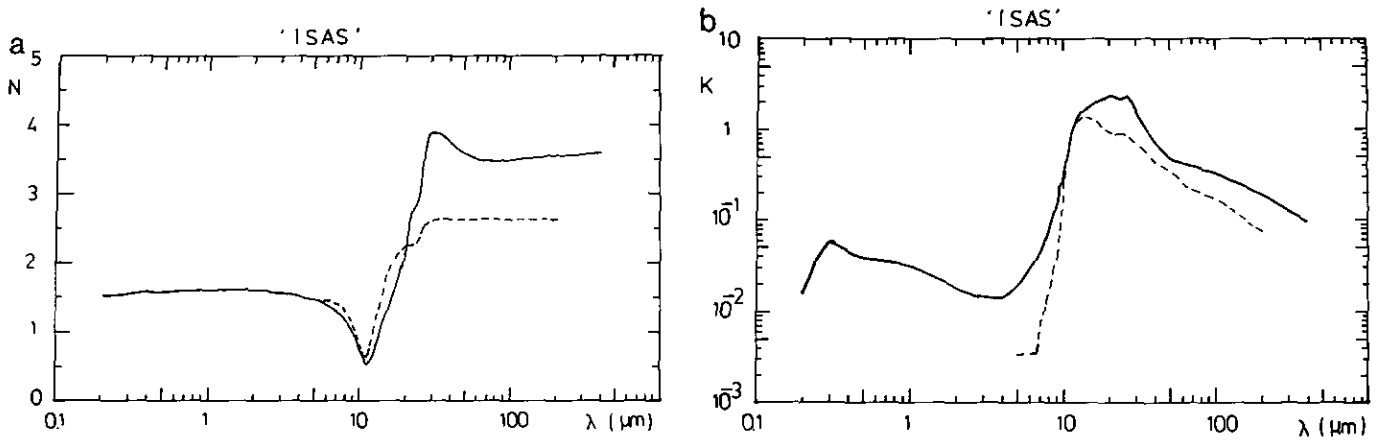

FIG. 8. The refractive indices n (a) and k (b) of γ-alumina particles obtained from combustion products particles (ISAS). Those of γ-alumina (Eriksson *et al.* 1981) are shown by the dashed curve.

sion showed a spherule composed of a corundum core surrounded by a mantle of hibonite and perovskite. The textural evidence indicates that corundum formed first and later reacted to produce hibonite (Bar-Mathews *et al.* 1982). Thus, high reactivity of corundum with the cooling gas may be related to the fact that corundum is exceedingly rare in meteorites.

Recently, 26 corundum (Al_2O_3) grains have been recovered from Murchison C2 chondrite, ranging in size from 3 to 15 μm (Anders *et al.* 1991, Virag *et al.* 1991). Furthermore, Al_2O_3 grains with large isotopic anomaly have been found from Orgueil and Bishnpur (Hutcheon *et al.* 1994, Huss *et al.* 1994). It is considered (Huss *et al.* 1994) that the Al_2O_3 grains formed in circumstellar environments of red giants and AGB stars because of their isotopic anomaly. Al_2O_3 grains at condensation from the gas may be γ-alumina, and many different species might occur through gas–solid reactions and accretion to meteorites. It is nec-

TABLE II
Alumina Dust in Space

Astronomical environment	Al_2O_3 found (d = size, λ = peak wavelength)		Reference
Meteorites			
Murchison C2	Physically	corundum-rich inclusion	Bar-Mathews et al. (1982)
	Physically	26 corundum grains ($d = 3 - 15\,\mu$m)	Anders et al. (1991) Virag (1991)
Orgueil CI	Physically	30 corundum grains	Hutcheon et al. (1994)
Bishunpur LL3.1	Physically	27 Al_2O_3 grains	Huss (1994)
IDPs	Physically	Alumina Oxide ($d = 3 - 8\,\mu$m) (contami from rockets ?)	Brownlee et al. (1976)
Lunar	Physically	α-corundum ($d = 40 - 100\,\mu$m)	Kleinman et al. (1971)
Miras	Spectroscopically	($\lambda = 12, 20\,\mu$m)	Vardya et al. (1986)
	Calculated feature	γ-alumina	Onaka et al. (1989)
Oxygen-rich stars	spectroscopically	metal oxides? ($\lambda = 7.15, 10, 11.5, 13.1, 18, 19.7\,\mu$m)	Goebel et al. (1994)
SN 1987A	Spectroscopically	unidentified	Bouchet et al. (1993)
	Condensation model	Al_2O_3	Kozasa et al. (1989, 1991)
Supernovae	Calculated feature	α-alumina ($\lambda = 12.7$ or $14\,\mu$m)	Pearce and Evans (1984)

essary to measure the spectra of these species for clarifying various processes from circumstellar condensation to accretion to form meteorites.

4.2. *Extraterrestrial Particles*

Only few alumina grains have been recovered from interplanetary dust particles (IDPs) collected by balloons and the U-2 aircraft (Brownlee *et al.* 1976). There is some contaminated by solid fuel rocket emissions (Brownlee *et al.* 1976); those grains exhibit shape similar to that of ISAS combustion particles shown in Fig. 2. It is difficult to distinguish the interplanetary dust grains from Al_2O_3 grain morphology alone.

As another type of sampled extraterrestrial grains, white grains with a bright luster were extracted from Apollo 11 fines (Kleinman and Ramdohr 1971). They were identified as α-corundum by X-ray diffraction and by electron microprobe analysis. It is believed that the α-corundum condensed from a vapor phase produced by an impact (Kleinman *et al.* 1971). If this is the case, it is expected that α-corundum may be found in IDPs, in circumstellar dust, etc.

4.3. *Mira Variables (Pulsating O-Rich Red Supergiants)*

Some M-type Mira variables show strong silicate emission features at 9.7 and 20 μm, while others show a rather flat spectrum with weaker broad emission features at 12 and 20 μm (Vardya *et al.* 1986). Equilibrium condensation calculations show that aluminum oxide is one of the first materials to condense in the expanding and cooling gas of cosmic composition. Onaka *et al.* (1989) have shown that the broad 12-μm feature observed can be reproduced by aluminum oxide grains. They adopted optical data of γ-aluminum oxide film (Eriksson *et al.* 1981). The resulting model feature was too sharp and too narrow compared with the observed spectra, and the peak positions occurred at wavelengths slightly shorter than those observed. The feature of the present ISAS, which has an absorption peak at a longer wavelength (12.1 μm) and with larger width than those of their adopted data (the Eriksson *et al.* γ-alumina), might give a better fit to the observed features than the Onaka *et al.* model. The dust particles present in Mira variables may be similar to those of the present ISAS. The quantitative comparison is left for future work.

Besides Mira variables, new emission features have been observed at 7.15-, 10-, 11.5-, 13.1-, 18-, and 19.7-μm bands in other oxygen-rich circumstellar shells (Goebel *et al.* 1994). These bands may originate from a series of bands due to various metal oxide condensates (Goebel *et al.* 1994). The observed 13.1-μm band appears to resemble to that of crystalline γ-alumina rather than amorphous γ-alumina, which has a band at about 11.8 μm in vacuum. On the other hand, the crystalline γ-alumina of ISAS has a broader band at 12.1 μm in vacuum than the observed 13.1-μm band.

4.4. *SN 1987A*

A theory of nonequilibrium nucleation and grain growth shows that Al_2O_3 grains are the first major condensate upon cooling of the ejecta of SN 1987A (Kozasa *et al.* 1989, 1991). Their radius is calculated to be typically $\sim$10 Å, whereas our Alumina grains have radii larger than this by an order of magnitude. It is not easily determined whether ultrafine particles of about 10 Å in size are amorphous or crystalline or whether they are α-alumina or γ-alumina. If the Al_2O_3 grains growing in the ejecta of SN 1987A are γ-alumina, the characteristic spectral feature might appear at about 12–13 μm. If they are α-alumina, the spectral feature might appear at 12.7, 15.9, 20.8, and 26 μm as shown in Pearce and Evans (1984). Roche *et al.* (1993) observed the spectra at 8–13 μm of SN 1987A, and found that the 3- to 13-μm dust emission spectrum between Days 465 and 578 is better fitted by grains with an emissivity law at least as λ^{-1}. Afterward, the 10-μm emission faded as the dust cooled. The dust emission spectrum showed no evidence of a strong spectral feature in the 8- to 13-μm region (Roche *et al.* 1993, Bouchet and Danzigar 1993). Timmermann and Larson (1993) pointed out that the missing band around 10 μm might have been suppressed by an IR echo emitted from circumstellar dust around SN 1987A. It is not obvious at present whether Al_2O_3 grains formed in the ejecta of SN 1987A and, if so, whether they are amorphous or crystalline or whether they are α-alumina or γ-alumina.

4.5. *Concluding Remarks*

It is not clear what type of crystalline structure of corundum is probable for circumstellar or interplanetary dust. Although corundum is the first major condensate of a gas of solar abundance, it is subsequently transformed, by reactions with gaseous Ca and Mg compounds, to spinel ($MgAl_2O_3$), hibonite ($CaAl_{12}O_{19}$), and other compounds at lower temperatures (Yamamoto and Hasegawa 1977). Therefore, corundum itself may be very difficult to observe or detect in circumstellar or interplanetary environments. We are presently studying the alteration processes by which corundum transforms to other phases.

APPENDIX

TABLE AI
The Refractive Indices of "Alumina" and "ISAS"

	'Alumina'		'ISAS'			'Alumina'		'ISAS'	
λ/μm	n	k	n	k	λ/μm	n	k	n	k
0.2			1.53	1.63(-2)	12.1	0.942	1.05	0.600	1.25
0.3			1.55	5.94(-2)	12.2	0.957	1.04	0.625	1.29
0.4			1.58	4.39(-2)	12.3	0.955	1.03	0.654	1.34
0.5	1.55	1.50(-2)	1.58	3.82(-2)	12.4	0.948	1.04	0.686	1.37
0.6	1.56	1.40(-2)	1.58	3.67(-2)	12.5	0.945	1.07	0.721	1.41
0.7	1.56	1.25(-2)	1.59	3.58(-2)	12.6	0.953	1.11	0.757	1.43
0.8	1.56	1.11(-2)	1.59	3.49(-2)	12.7	0.977	1.14	0.792	1.45
0.9	1.56	9.86(-3)	1.59	3.37(-2)	12.8	1.02	1.18	0.824	1.47
1.0	1.56	8.88(-3)	1.60	3.19(-2)	12.9	1.06	1.19	0.851	1.48
2.0	1.55	4.92(-3)	1.59	1.81(-2)	13.0	1.11	1.19	0.873	1.49
3.0	1.53	5.12(-3)	1.57	1.40(-2)	13.1	1.14	1.17	0.891	1.50
4.0	1.50	7.44(-3)	1.53	1.43(-2)	13.2	1.15	1.15	0.907	1.52
5.0	1.46	1.14(-2)	1.47	1.83(-2)	13.3	1.15	1.14	0.921	1.54
6.0	1.41	1.83(-2)	1.40	2.72(-2)	13.4	1.14	1.14	0.937	1.56
7.0	1.33	3.05(-2)	1.30	4.41(-2)	13.5	1.13	1.15	0.953	1.58
8.0	1.23	5.23(-2)	1.17	7.59(-2)	13.6	1.13	1.17	0.972	1.60
9.0	1.09	9.44(-2)	0.980	1.44(-1)	13.7	1.13	1.19	0.992	1.62
10.0	0.880	1.95(-1)	0.735	3.06(-1)	13.8	1.14	1.21	1.01	1.64
10.1	0.852	2.13(-1)	0.704	3.34(-1)	13.9	1.15	1.24	1.04	1.66
10.2	0.823	2.34(-1)	0.674	3.66(-1)	14.0	1.17	1.26	1.06	1.67
10.3	0.793	2.57(-1)	0.646	4.01(-1)	14.1	1.20	1.28	1.08	1.69
10.4	0.763	2.85(-1)	0.619	4.40(-1)	14.2	1.22	1.30	1.11	1.70
10.5	0.731	3.16(-1)	0.594	4.81(-1)	14.3	1.25	1.31	1.13	1.71
10.6	0.700	3.53(-1)	0.573	5.26(-1)	14.4	1.28	1.31	1.15	1.72
10.7	0.670	3.95(-1)	0.555	5.72(-1)	14.5	1.30	1.31	1.17	1.73
10.8	0.643	4.43(-1)	0.540	6.19(-1)	14.6	1.33	1.31	1.19	1.74
10.9	0.619	4.97(-1)	0.528	6.68(-1)	14.7	1.35	1.30	1.20	1.75
11.0	0.601	5.56(-1)	0.520	7.17(-1)	14.8	1.37	1.29	1.22	1.76
11.1	0.590	6.20(-1)	0.514	7.66(-1)	14.9	1.38	1.28	1.23	1.77
11.2	0.586	6.86(-1)	0.511	8.16(-1)	15.0	1.39	1.27	1.25	1.78
11.3	0.591	7.56(-1)	0.511	8.65(-1)	15.1	1.39	1.26	1.26	1.79
11.4	0.607	8.25(-1)	0.513	9.14(-1)	15.2	1.40	1.25	1.27	1.80
11.5	0.633	8.94(-1)	0.518	9.63(-1)	15.3	1.39	1.24	1.28	1.81
11.6	0.672	9.58(-1)	0.525	1.01	15.4	1.39	1.24	1.30	1.83
11.7	0.723	1.01	0.534	1.06	15.5	1.38	1.24	1.31	1.84
11.8	0.785	1.05	0.546	1.11	15.6	1.37	1.24	1.32	1.86
11.9	0.849	1.07	0.561	1.16	15.7	1.36	1.24	1.34	1.87
12.0	0.905	1.07	0.579	1.20	15.8	1.35	1.25	1.35	1.89

TABLE AI—*Continued*

	'Alumina'		'ISAS'			'Alumina'		'ISAS'	
λ/μm	n	k	n	k	λ/μm	n	k	n	k
15.9	1.34	1.26	1.37	1.90	20.1	2.28	2.15	2.19	2.35
16.0	1.33	1.27	1.39	1.92	20.2	2.33	2.14	2.22	2.35
16.1	1.32	1.29	1.41	1.94	20.3	2.38	2.12	2.25	2.35
16.2	1.31	1.31	1.42	1.95	20.4	2.43	2.10	2.27	2.35
16.3	1.30	1.33	1.45	1.96	20.5	2.48	2.08	2.30	2.35
16.4	1.30	1.35	1.47	1.98	20.6	2.52	2.05	2.33	2.35
16.5	1.29	1.38	1.49	1.99	20.7	2.56	2.02	2.35	2.35
16.6	1.29	1.40	1.51	2.00	20.8	2.60	1.99	2.38	2.34
16.7	1.29	1.43	1.53	2.01	20.9	2.64	1.95	2.40	2.34
16.8	1.30	1.46	1.55	2.02	21.0	2.67	1.92	2.43	2.34
16.9	1.30	1.48	1.57	2.02	21.1	2.70	1.88	2.46	2.33
17.0	1.31	1.51	1.59	2.03	21.2	2.72	1.85	2.48	2.33
17.1	1.31	1.54	1.61	2.03	21.3	2.74	1.81	2.50	2.32
17.2	1.32	1.57	1.62	2.04	21.4	2.76	1.77	2.53	2.31
17.3	1.33	1.59	1.64	2.05	21.5	2.77	1.74	2.55	2.31
17.4	1.34	1.62	1.66	2.05	21.6	2.78	1.70	2.57	2.30
17.5	1.36	1.65	1.67	2.06	21.7	2.79	1.67	2.60	2.29
17.6	1.37	1.68	1.68	2.06	21.8	2.80	1.63	2.62	2.28
17.7	1.39	1.71	1.70	2.07	21.9	2.81	1.60	2.64	2.27
17.8	1.40	1.73	1.71	2.08	22.0	2.81	1.57	2.66	2.25
17.9	1.42	1.76	1.72	2.09	22.1	2.81	1.54	2.67	2.24
18.0	1.44	1.79	1.73	2.10	22.2	2.81	1.52	2.69	2.23
18.1	1.46	1.82	1.74	2.11	22.3	2.81	1.49	2.71	2.22
18.2	1.48	1.85	1.76	2.12	22.4	2.81	1.47	2.72	2.20
18.3	1.51	1.88	1.77	2.14	22.5	2.80	1.44	2.73	2.19
18.4	1.53	1.91	1.78	2.15	22.6	2.80	1.42	2.74	2.18
18.5	1.56	1.93	1.80	2.17	22.7	2.79	1.40	2.75	2.17
18.6	1.59	1.96	1.81	2.18	22.8	2.79	1.38	2.76	2.16
18.7	1.62	1.99	1.83	2.20	22.9	2.78	1.37	2.77	2.15
18.8	1.66	2.02	1.85	2.21	23.0	2.77	1.35	2.77	2.14
18.9	1.70	2.04	1.87	2.23	23.1	2.77	1.34	2.78	2.13
19.0	1.74	2.06	1.89	2.24	23.2	2.76	1.32	2.78	2.13
19.1	1.78	2.09	1.92	2.26	23.3	2.75	1.31	2.78	2.12
19.2	1.82	2.11	1.94	2.27	23.4	2.75	1.30	2.79	2.12
19.3	1.87	2.12	1.97	2.29	23.5	2.74	1.29	2.79	2.11
19.4	1.92	2.14	1.99	2.30	23.6	2.73	1.28	2.79	2.11
19.5	1.97	2.15	2.02	2.31	23.7	2.73	1.27	2.80	2.11
19.6	2.02	2.16	2.05	2.32	23.8	2.72	1.27	2.80	2.12
19.7	2.07	2.17	2.08	2.33	23.9	2.71	1.26	2.80	2.12
19.8	2.12	2.17	2.10	2.33	24.0	2.71	1.26	2.81	2.12
19.9	2.18	2.17	2.13	2.34	24.1	2.70	1.25	2.81	2.13
20.0	2.23	2.16	2.16	2.34	24.2	2.70	1.25	2.82	2.14

ACKNOWLEDGMENTS

We thank Prof. H. Okuda of ISAS for helping us with the far-infrared extinction measurements. This work was supported by ISAS. We thank Drs. J. H. Goebel and J. Mathis for improvement of the original manuscript.

REFERENCES

ANDERS, E., A. VIRAG, E. ZINNER, AND R. S. LEWIS 1991. ^{26}Al and ^{16}O in the early solar system: Clues from meteoritic Al_2O_3. *Astrophys. J.* **373,** L77–L80.

BARKER, A. S., JR. 1963. Infrared lattice vibrations and dielectric dispersion in corundum. *Phys. Rev.* **132,** 1474–1481.

BAR-MATTHEWS, M., I. D. HUTCHEON, G. J. MACPHERSON, AND L. GROSSMAN 1982. A corundum-rich inclusion in the Murchison carbonaceous chondrite. *Geochim. Cosmochim. Acta* **46,** 31–41.

BOUCHET, P., AND I. J. DANZIGAR 1993. Infrared photometry and spectrophotometry of SN 1987A. II. November 1987 to March 1991 observations. *Astron. Astrophys.* **273,** 451–472.

BROWNLEE, D. E., G. V. FERRY, AND D. TOMANDL 1976. Stratospheric aluminum oxide. *Science* **191,** 1270–1271.

ERIKSSON, T. S., A. HJORTSBERG, G. A. NIKLASSON, AND C. G. GRANQVIST 1981. Infrared optical properties of evaporated alumina films. *Appl. Opt.* **20,** 2742–2746.

GOEBEL, J. H., J. D. BREGMAN, AND F. C. WITTEBORN 1994. A 7 micron dust emission feature in oxygen-rich circumstellar shells. *Astrophys. J.* **430,** 317–322.

GROSSMAN, L. 1972. Condensation in the primitive solar nebula. *Geochim. Cosmochim. Acta* **36,** 597–619.

HEATON, H. I. 1971. Infrared refractive indices of alkali halides. *J. Opt. Soc. Am.* **61,** 275–276.

HUSS, G. R., A. J. FAHEY, R. GALLINO, AND G. J. WASSERBURG 1994. Oxygen isotopes in circumstellar Al_2O_3 grains from meteorites and stellar nucleosynthesis. *Astrophys. J.* **430,** L81–L84.

HUTCHEON, I. D., G. R. HUSS, A. J. FAHEY, AND G. J. WASSERBURG 1994. Extreme ^{26}Mg and ^{17}O enrichments in an Orgueil corundum: Identification of a presolar oxide grain. *Astrophys. J.* **425,** L97–L100.

KLEINMANN, B., AND P. RAMDOHR 1971. Alpha-corundum from the lunar dust. *Earth Planet. Sci. Lett.* **13,** 19–22.

TABLE AI—*Continued*

	'Alumina'		'ISAS'			'Alumina'		'ISAS'	
λ/μm	n	k	n	k	λ/μm	n	k	n	k
24.3	2.69	1.24	2.83	2.14	28.4	2.82	1.26	3.76	1.92
24.4	2.69	1.24	2.84	2.15	28.5	2.82	1.26	3.78	1.90
24.5	2.68	1.24	2.85	2.16	28.6	2.83	1.26	3.79	1.88
24.6	2.68	1.24	2.86	2.17	28.7	2.84	1.25	3.80	1.85
24.7	2.68	1.24	2.87	2.18	28.8	2.85	1.25	3.81	1.83
24.8	2.68	1.24	2.88	2.19	28.9	2.86	1.25	3.82	1.81
24.9	2.67	1.24	2.90	2.20	29.0	2.86	1.25	3.83	1.79
25.0	2.67	1.24	2.92	2.21	29.1	2.87	1.24	3.83	1.76
25.1	2.67	1.24	2.94	2.22	29.2	2.88	1.24	3.84	1.74
25.2	2.67	1.24	2.95	2.23	29.3	2.89	1.24	3.85	1.72
25.3	2.67	1.24	2.98	2.24	29.4	2.89	1.24	3.85	1.70
25.4	2.67	1.24	3.00	2.25	29.5	2.90	1.23	3.85	1.68
25.5	2.67	1.24	3.02	2.26	29.6	2.91	1.23	3.86	1.66
25.6	2.67	1.24	3.05	2.26	29.7	2.92	1.22	3.86	1.64
25.7	2.67	1.24	3.07	2.27	29.8	2.92	1.22	3.86	1.62
25.8	2.67	1.24	3.10	2.27	29.9	2.93	1.22	3.87	1.60
25.9	2.68	1.25	3.13	2.28	30.0	2.94	1.21	3.87	1.58
26.0	2.68	1.25	3.16	2.28	30.5	2.98	1.19	3.87	1.50
26.1	2.68	1.25	3.19	2.28	31.0	3.01	1.16	3.87	1.43
26.2	2.68	1.25	3.22	2.28	31.5	3.04	1.13	3.87	1.36
26.3	2.69	1.25	3.25	2.28	32.0	3.07	1.10	3.87	1.30
26.4	2.69	1.25	3.28	2.27	32.5	3.09	1.07	3.87	1.25
26.5	2.69	1.26	3.31	2.27	33.0	3.11	1.03	3.86	1.20
26.6	2.70	1.26	3.34	2.26	34.0	3.14	0.969	3.85	1.11
26.7	2.70	1.26	3.37	2.25	35.0	3.16	0.905	3.84	1.03
26.8	2.71	1.26	3.40	2.24	36.0	3.18	0.845	3.83	0.953
26.9	2.71	1.26	3.43	2.23	37.0	3.18	0.790	3.81	0.886
27.0	2.72	1.26	3.46	2.21	38.0	3.19	0.739	3.79	0.826
27.1	2.73	1.26	3.49	2.20	39.0	3.18	0.693	3.77	0.774
27.2	2.73	1.26	3.52	2.18	40.0	3.18	0.651	3.75	0.728
27.3	2.74	1.26	3.55	2.16	41.0	3.17	0.614	3.73	0.688
27.4	2.74	1.27	3.57	2.15	42.0	3.17	0.580	3.71	0.653
27.5	2.75	1.27	3.60	2.13	43.0	3.16	0.550	3.69	0.622
27.6	2.76	1.27	3.62	2.11	44.0	3.15	0.522	3.67	0.596
27.7	2.76	1.27	3.64	2.08	45.0	3.14	0.497	3.65	0.572
27.8	2.77	1.27	3.66	2.06	46.0	3.13	0.475	3.63	0.552
27.9	2.78	1.27	3.68	2.04	47.0	3.12	0.455	3.61	0.535
28.0	2.79	1.26	3.70	2.02	48.0	3.11	0.436	3.60	0.519
28.1	2.79	1.26	3.72	1.99	49.0	3.11	0.419	3.59	0.505
28.2	2.80	1.26	3.74	1.97	50.0	3.10	0.404	3.57	0.493
28.3	2.81	1.26	3.75	1.95	55.0	3.06	0.345	3.52	0.450

TABLE AI—*Continued*

	'Alumina'		'ISAS'			'Alumina'		'ISAS'	
λ/μm	n	k	n	k	λ/μm	n	k	n	k
60.0	3.03	0.308	3.50	0.424	160	2.95	0.160	3.53	0.230
65.0	3.00	0.285	3.48	0.406	170	2.95	0.164	3.54	0.218
70.0	2.99	0.273	3.47	0.392	180	2.95	0.168	3.54	0.207
75.0	2.98	0.264	3.47	0.380	190	2.95	0.173	3.55	0.197
80.0	2.98	0.255	3.47	0.369	200	2.96	0.177	3.55	0.188
85.0	2.99	0.243	3.47	0.358	220	2.97	0.182	3.55	0.173
90.0	2.99	0.228	3.48	0.347	240	2.99	0.183	3.56	0.159
95.0	2.99	0.214	3.48	0.337	260	3.01	0.180	3.56	0.148
100	2.99	0.200	3.49	0.327	280	3.02	0.173	3.56	0.137
110	2.98	0.180	3.50	0.307	300	3.03	0.166	3.56	0.129
120	2.97	0.167	3.51	0.289	325	3.04	0.155	3.56	0.119
130	2.96	0.160	3.52	0.272	350	3.05	0.144	3.57	0.111
140	2.95	0.157	3.52	0.257	375	3.06	0.135	3.57	0.104
150	2.95	0.158	3.53	0.243	400	3.06	0.126	3.57	9.72(-2)

Note. 1.63(-2), for example, means 1.63×10^{-2}

TABLE AII

The Refractive Indices of Amorphous γ-Alumina (Eriksson *et al.* 1981)

λ/μm	n	k
5.00	1.48	3.37(-3)
6.67	1.43	3.49(-3)
6.90	1.41	5.30(-3)
7.14	1.40	7.14(-3)
7.41	1.37	9.12(-3)
7.69	1.34	1.12(-2)
8.00	1.30	1.53(-2)
8.33	1.28	1.95(-2)
8.70	1.18	2.96(-2)
9.09	1.05	3.81(-2)
9.52	1.00	7.48(-2)
10.0	0.826	0.182
10.5	0.661	0.454
11.1	0.635	0.709
11.8	0.806	1.02
12.5	1.03	1.26
13.3	1.30	1.38
14.3	1.55	1.38
15.4	1.81	1.33
15.9	1.93	1.27
16.7	2.01	1.20
18.2	2.13	1.03
20.0	2.25	0.923
21.6	2.25	0.891
22.2	2.25	0.891
23.3	2.27	0.915
25.0	2.33	0.912
26.4	2.53	0.849
28.6	2.58	0.743
33.3	2.62	0.572
40.0	2.63	0.438
50.0	2.62	0.343
66.7	2.63	0.219
100.0	2.63	0.171
200.0	2.64	7.58(-2)

KOIKE, C., H. HASEGAWA, N. ASADA, AND T. HATTORI 1981. The extinction coefficients in mid- and far-infrared of silicate and iron-oxide minerals of interest for astronomical observations. *Astrophys. Space Sci.* **79,** 77–85.

KOIKE, C., H. HASEGAWA, N. ASADA, AND T. KOMATUZAKI 1989. Optical constants of fine particles for the infrared region. *Mon. Not. R. Astron. Sci.* **239,** 127–137.

KOIKE, C., AND H. SHIBAI 1994. Mid- and far-infrared absorption spectra of fine fused quartz grains. *Mon. Not. R. Astron. Sci.* **269,** 1011–1018.

KORNACKI, A. S., AND B. FEGLEY, JR. 1984. Origin of spinel-rich chondrules and inclusions in carbonaceous and ordinary chondrites. *J. Geophys. Res.* **89,** B588–B596.

KOZASA, T., H. HASEGAWA, AND K. NOMOTO 1989. Formation of dust grains in the ejecta of SN 1987A. *Astrophys. J.* **344,** 325–331.

KOZASA, T., H. HASEGAWA, AND K. NOMOTO 1991. Formation of dust grains in the ejecta of SN 1987A. II. *Astron. Astrophys.* **249,** 474–482.

MITUISHI, A., Y. YAMADA, S. FUJITA, AND H. YOSHINAGA 1960. Polarizer for the far-infrared region. *J. Opt. Soc. Am.* **50,** 433–436.

ONAKA, T., T. DE JONG, AND F. J. WILLEMS 1989. A study of M Mira variables based on IRAS LRS observations. I. Dust formation in the circumstellar shell. *Astron. Astrophys.* **218,** 169–179.

PEARCE, G., AND A. EVANS 1984. The infra-red emission from a composite circumstellar dust shell heated by a supernova. *Astron. Astrophys.* **136,** 306–312.

POLLACK, J. B., O. B. TOON, AND B. N. KHARE 1973. Optical properties of some terrestrial rocks and glasses. *Icarus* **19,** 372–389.

ROCHE, P. F., D. K. AITKEN, AND C. H. SMITH 1993. The evolution of the 8–13 μm spectrum of supernova 1987A. *Mon. Not. R. Astron. Sci.* **261,** 522–534.

SUTO, H., C. KOIKE, AND H. SHIBAI 1992. Comparison of approximation methods with the measurements of extinction of fine particles in the infrared region. *Proceedings of the 25th ISAS Lunar and Planetary Symposium* **25,** 262–267.

TANABE, K., T. SEIYAMA, AND K. FUEKI 1993. Al oxides. In *Metal Oxides and Compound Oxides* Chap. 6, pp. 72–86. Kodansya, Japan. (K. Tanabe, T. Seiyama and K. Fueki, Eds.), [in Japanese]

TIMMERMANN, R., AND H. P. LARSON 1993. Evidence for hydrated silicates toward SN 1987A. *Astrophys. J.* **415,** 820–831.

TOON, O. B., AND J. B. POLLACK 1976. The optical constants of several atmospheric aerosol species: Ammonium sulfate, aluminum oxide, and sodium chloride. *J. Geophys. Res.* **81,** 5733–5748.

VARDYA, M. S., T. DE JONG, AND F. J. WILLEMS 1986. IRAS Low-Resolution spectrograph observations of silicate and molecular SiO emission in Mira variables. *Astrophys. J.* **304,** L29–L32.

VIRAG, A., E. ZINNER, S. AMARI, AND E. ANDERS 1991. An ion microprobe study of corundum in the Murchison meteorite: Implications for ^{26}Al and ^{16}O in the early solar system. *Geochim. Cosmochim. Acta* **55,** 2045–2062.

YAMAMOTO, T., AND H. HASEGAWA 1977. Grain Formation through nucleation process in astrophysical environment. *Prog. Theor. Phys.* **58,** 816–828.